



Numerical Analysis of Edge Deformation and Force via Continuous Function Curves in Vertical Rolling Process

Boxin Yang¹ · Haojie Xu² · Qi An¹

Received: 22 June 2023 / Accepted: 8 September 2023 / Published online: 27 October 2023
© The Author(s), under exclusive licence to Shiraz University 2023

Abstract

Vertical rolling is usually arranged before horizontal rolling in continuous hot rolling to control the width precision and improve the process quality. Due to the complicated contact and deformation rule, it is significant to establish a method to accurately calculate rolling force and edge deformation. A continuous functions model is proposed to describe the edge deformation, and the velocity and strain rate fields are derived according to the properties of stream function. The adhesion of the contact interface is successfully considered in the analysis of friction. By using Mises yield criterion and Pavlov projection principle, the total power functional is obtained. The vertical rolling force and plastic deformation are calculated by the theory of energy minimization, and the result is well verified by specific examples. The effects of equipment parameters and slab size on rolling force, rolling power and edge deformation are analyzed. The proposed mathematical model successfully applies functional analysis to the engineering field, which is helpful for controlling slab shape and optimizing vertical rolling process.

Keywords Vertical rolling process · Rolling force · Edge deformation · Energy method · Functional analysis

1 Introduction

In roughing rolling stage, vertical rolling is usually arranged before plain rolling to control the width precision and restrain the non-rectangularization of slab. During rolling, the deformation (dog-bone deformation) only occurs at the slab edge, and the deformation law is very complex. Theoretical research on metal forming process has been proven to be of great significance in improving production yield and quality (Bari and Kumar 2023a). Therefore, in-depth research on vertical rolling process is necessary.

Scholars have conducted several experimental research on vertical rolling process. Okado et al. (1981) simulated vertical rolling by pure lead and firstly proposed the empirical formulas of four deformation parameters (peak height, peak position, edge thickness and deformation length) to describe the dog-bone shape. Shibahara et al. (1981) built

a vertical rolling model through the regression analysis of measured value. Based on Shibahara's results, Tazoe et al. (1984) obtained an empirical formula of peak height and pointed out that the dog-bone length and the peak position are directly proportion to width reduction. Later, the formula was modified by Ginzburg et al. (1991), and the result is consistent with the plastic mud model put forward by Huisman and Huëtink (1985). Xiong et al. (1997) developed a vertical rolling experiment with the simulation ratio of 10. The fitted dog-bone formulas consider the width reduction, roller diameter, initial slab thickness and width. However, the results are greatly affected by experimental conditions.

With the widespread popularity of computer technology, the simulation of vertical rolling process is carried out by finite element software. Xiong et al. (2003) obtained the friction characteristics of 3D contact based on micro-compressible plastic theory and the simplified Euler formula. By using 3D elastic–viscoplastic FEM, Forouzan et al. (2009) studied the sizing press and vertical rolling under heavy width reduction. The influences of slab size and width reduction on edge deformation and the head and end quality of slab were studied. Ruan et al. (2014) used a 3D thermo-mechanical coupled rigid–plastic FEM to analyze the non-rectangular shape and the evolution rules of wide and heavy plate in hot rolling process.

✉ Qi An
anqi@ecust.edu.cn

¹ School of Mechanical and Power Engineering, East China University of Science and Technology, Shanghai 200237, People's Republic of China

² Yangtze Delta Region Institute of Tsinghua University, Jiaxing 314000, Zhejiang, People's Republic of China

Theoretical researches have been carried out later. Based on plane deformation assumption, Lundberg (1986; 2008) and Lundberg and Gustafsson (1993) established a triangular velocity field of vertical rolling process considering friction and smoothness condition, respectively. Then, the hodograph of plastic flow and the torque formulas were obtained. Zhang et al. (2018; 2020) drew the slip line field and hodograph of edge deformation zone under full adhesive contact, and the analytical solutions of mechanics parameters and dog-bone shape were deduced. Yun et al. (2012) assumed that the deformation was distributed in the entire width and then established a theoretical model with several power functions. Meanwhile, some deformation parameters and rolling force were fitted according to FEM result. But the slope growth of the high-power function is too fast, so the predicted deformation zone of the dog-bone is often too wide. Li et al. (2016) established an upper bound power functional for edge rolling by using complex mathematical functions. The edge rolling force and torque are calculated by minimizing the power functional. Cao et al. (2016) used sine function to describe edge deformation and established the energy model by stream function method. Simplifying the peak position and the dog-bone length as 1:3 as well as full sliding assumption of the contact interface, Liu et al. (2015; 2016) deduced the total power functional. However, the dog-bone shapes are more concentrate at the edge, which result in the higher dog-bone peak and the predicted rolling force. Later, Liu et al. (2020; 2022) built double stream function velocity fields to build the numerical and analytical model.

Through the analysis of the above studies, the research on vertical rolling force and edge deformation is still insufficient. The predicted force and shape are quite different and cannot be in good agreement with measurements (Yun et al. 2012; Liu et al. 2016). The difficulty of energy method in vertical rolling process is to choose suitable deformation curves and kinematically admissible velocity field. In this paper, cubic function is combined with gamma distribution function to form the edge deformation model. The velocity and strain rate fields are built based on stream function method. The plastic deformation power and inlet shear power are calculated based on Mises yield criterion and the velocity discontinuity. After fully considering the adhesion of the contact interface, the friction power is calculated by using inner product of collinear principle. The total power functional is derived based on the new method. Then, the calculated edge shape and rolling force are compared with other results, which verified the precision of the proposed method. Finally, the effects of slab and equipment parameters on mechanical properties and edge deformation are studied.

2 Mechanics Model of Vertical Rolling Process

2.1 Vertical–Horizontal Rolling Process

The basic process of continuous hot rolling is shown in Fig. 1. The vertical rollers are driven by motors with a constant speed ω_v . The steel slab moves forward and passes through the clearance between a pair of vertical rollers at the initial velocity v_0 . Under the extrusion of the vertical rollers, the slab width reduces from W_0 to W_1 . Then the slab is rolled by a pair of horizontal rollers. The slab length increases with the decrease in thickness under the compression plastic deformation.

2.2 Edge Deformation Model

As shown in Fig. 2, the steel slab occurs non-uniform plastic deformation when rolled by vertical rollers. For the high ratio of width to thickness, the deformation is mainly restricted at the edge with obvious bulge in the thickness direction. Finally, the dog-bone deformation is formed, which is exhibited in Fig. 2.

Before analyzing, the assumptions are given as follows:

(1) The microstructure of steel slab and vertical rollers is uniform and isotropic. (2) The vertical rollers are rigid bodies. (3) The elastic deformation of the steel slab is ignored. The tension and width lose are ignored. (4) The force and plastic deformation rules of the steel slab are symmetrical. So, a quarter of the deformation zone is analyzed.

As shown in Fig. 2a, the center of entrance cross section is selected as the coordinate origin to establish a three-dimensional coordinate system. H_0 represents the initial thickness of steel slab. W_0 and W_1 represent the slab width before and after rolling, respectively. The unilateral reduction $\Delta w = \frac{\Delta W}{2} = \frac{W_0 - W_1}{2}$. R represents the vertical roller radius. The projected length of the roller–slab contact arc in

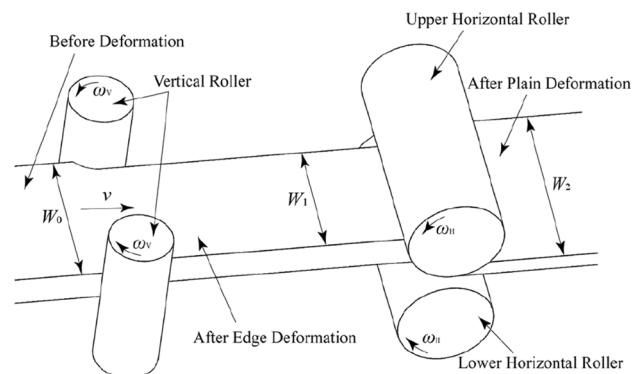
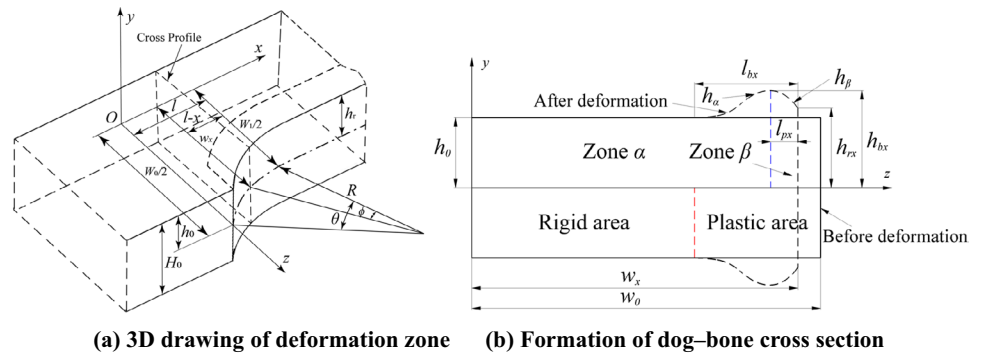


Fig. 1 Continuous hot rolling process

Fig. 2 Plastic deformation in vertical rolling process



rolling direction is $l = R \sin \theta$. The bite angle is given by $\theta = \cos^{-1} \left(\frac{R - \Delta w}{R} \right)$. Half of the width and half of the width reduction at any position are $w_x = \frac{w_0}{2} + R - \sqrt{R^2 - (l - x)^2}$ and $\Delta w_x = \frac{w_0}{2} - w_x$. The contact angle ϕ has the following relationship with x direction:

$$\phi = \sin^{-1} \left(\frac{l - x}{R} \right)$$

$$d\phi = -\frac{dx}{R \cos \phi}$$

The first- and second-order derivative equations of w_x are:

$$w'_x = -\frac{l - x}{\sqrt{R^2 - (l - x)^2}} = -\tan \phi$$

$$w''_x = \frac{R^2}{[R^2 - (l - x)^2]^{\frac{3}{2}}}$$

Half of the thickness is denoted by $h(x, z)$. On arbitrary cross section along rolling direction, the height and position of dog-bone peak are expressed by h_{bx} and l_{px} , respectively. The height of dog-bone edge is expressed by h_{rx} . The length of dog-bone zone (plastic deformation zone) is expressed by l_{bx} , respectively.

In order to describe and analyze the edge deformation, it is essential to use appropriate functions to describe the edge shape of slab. In this paper, the dog-bone peak is used as the boundary, and the bite zone is divided into zone α and zone β .

Gamma distribution function in statistics is the product of power function and exponential function. It has both extreme value and the property of exponential function and can well describe the slow change of thickness between dog-bone peak and rigid zone. Thus, in zone α ($0 < z < w_x - l_{px}$), half of the slab thickness is expressed as:

$$h_\alpha = h_0 + \frac{ah_0 \Delta w_x}{l_{px}} \left(\frac{w_x - z}{l_{px}} \right)^2 e^{-2 \left(\frac{w_x - z}{l_{px}} \right)} \quad (1)$$

The cubic curve function has a simple form and is easy to integrate. It has been applied to describe the edge

deformation of vertical rolling process and has been proven to have high accuracy (Liu et al. 2022). In zone β ($w_x - l_{px} < z < w_x$), half of the slab thickness is expressed by cubic function:

$$h_\beta = h_0 + \frac{ah_0 \Delta w_x}{e^2 l_{px}} - \frac{bc_m h_0 \Delta w_x}{l_{px}} \left[2 \left(\frac{w_x - z}{l_{px}} \right)^3 - 3 \left(\frac{w_x - z}{l_{px}} \right)^2 + 1 \right] \quad (2)$$

where a and b are the undetermined parameters, c_m is the coefficient related to friction factor m

In previous researches, the friction factor of roller–slab contact is generally between 0.2 and 0.8, and the calculated $(h_r - h_0) / (h_b - h_0)$ is 0.3–0.75 (Okado et al. 1981; Xiong et al. 1997; Shibahara et al. 1981). According to the relationship between the friction factor and $(h_r - h_0) / (h_b - h_0)$, a simplified rule is assumed as:

$$c_m = \begin{cases} -2 \left(m - \frac{1}{2} \right)^2 + \frac{1}{2} & m \in \left(0, \frac{1}{2} \right) \\ 2 \left(m - \frac{1}{2} \right)^2 + \frac{1}{2} & m \in \left(\frac{1}{2}, 1 \right) \end{cases} \quad (3)$$

When the friction factor $m = 1$, the slab and the vertical roller are in full adhesion without any relative sliding, that is $c_m = 0$. Substituting into Eq. (2) yields:

$$b = \frac{a}{e^2}$$

According to plane deformation assumption and constant volume, the FEM established by Yun et al. (2012) shows that the maximum variation is less than 3%. Thus, in every cross section, there is:

$$\Delta w_x h_0 = \int_0^{w_x - l_{px}} (h_\alpha - h_0) dz + \int_{w_x - l_{px}}^{w_x} (h_\beta - h_0) dz \quad (4)$$

Substituting Eqs. (1) and (2) and the coefficient b into Eq. (4), there is:

$$a = \frac{4e^2}{9 - 2c_m}$$

Then, the expressions of dog-bone model can be written as follows:

$$h_\alpha = h_0 + \frac{4e^2 h_0 \Delta w_x}{(9 - 2c_m) l_{px}} \left(\frac{w_x - z}{l_{px}} \right)^2 e^{-2 \left(\frac{w_x - z}{l_{px}} \right)} \quad (5)$$

$$h_\beta = h_0 + \frac{4h_0 \Delta w_x}{(9 - 2c_m) l_{px}} - \frac{4c_m h_0 \Delta w_x}{(9 - 2c_m) l_{px}} \left[2 \left(\frac{w_x - z}{l_{px}} \right)^3 - 3 \left(\frac{w_x - z}{l_{px}} \right)^2 + 1 \right] \quad (6)$$

Then, the dog-bone deformation model only contains one unknown parameter l_{px} . For edge rolling process, the peak position of dog-bone l_{px} in bite zone can be simplified as a constant (Yun et al. 2012).

2.3 Velocity Field and Strain Rate Field of Plastic Flow

The stream function method is widely used to analyze plastic deformation. The premise of this method is the principle of volume invariance. Firstly, a differential equilibrium equation is established based on the relationship between volume flow components, and then the plastic flow field is determined through integration and the boundary conditions. The plastic flow in bite zone is shown in Fig. 3. ds and dS represent the front and back lateral width of the infinitesimal element in length direction, respectively, and $w(x, z)$ represents the function of lateral displacement.

According to the properties of stream function:

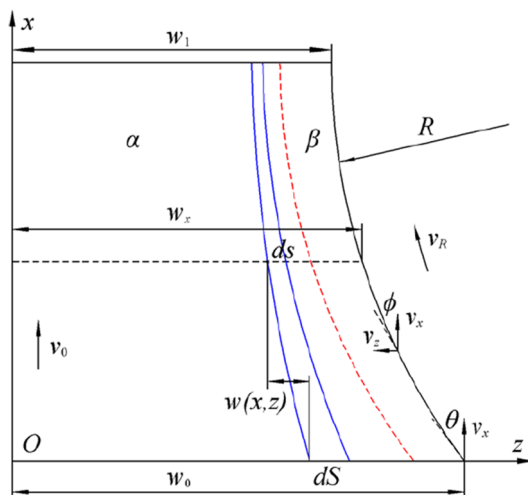


Fig. 3 Plastic flow diagram

$$\frac{\partial w}{\partial z} = \frac{ds - dS}{dS} \quad (7)$$

Based on the incompressibility of plastic flow, the speed in rolling direction is:

$$v_x = \frac{v_0 h_0}{h} \frac{dS}{ds} \quad (8)$$

Substituting Eq. (8) into Eq. (7), and considering when $\frac{\partial w}{\partial z} \ll 1$, $\frac{\partial w / \partial z}{1 + \partial w / \partial z} \approx \frac{\partial w}{\partial z}$, then:

$$v_x = \frac{v_0 h_0}{h} \left(1 - \frac{\partial w}{\partial z} \right) \quad (9)$$

The velocity in rolling direction and width direction has the following relationship:

$$\frac{v_z}{v_x} = \frac{\partial w}{\partial x} \quad (10)$$

Substituting Eq. (9) into Eq. (10) yields:

$$v_z = \frac{v_0 h_0}{h} \left(1 - \frac{\partial w}{\partial z} \right) \frac{\partial w}{\partial x} \quad (11)$$

According to Cauchy equation:

$$\dot{\epsilon}_y = \frac{\partial v_y}{\partial y} = -\frac{\partial v_x}{\partial x} - \frac{\partial v_z}{\partial z} \quad (12)$$

Substituting Eqs. (9) and (11) into Eq. (12) and noticing when $y = 0$, $v_y = 0$, the velocity in thickness direction can be obtained by solving the differential equation:

$$v_y = v_0 h_0 y \left\{ \left(\frac{\partial w}{\partial z} - 1 \right) \left[\frac{\partial}{\partial x} \left(\frac{1}{h} \right) + \frac{\partial}{\partial z} \left(\frac{1}{h} \right) \frac{\partial w}{\partial x} \right] + \frac{1}{h} \left(\frac{\partial w}{\partial z} \frac{\partial^2 w}{\partial x \partial z} + \frac{\partial w}{\partial x} \frac{\partial^2 w}{\partial z^2} \right) \right\} \quad (13)$$

For vertical rolling, the rolling velocity can be approximately regarded as constant:

$$v_x = v_0 \quad (14)$$

The lateral displacement can be obtained by substituting Eq. (14) into Eq. (9):

$$w = \int_0^z \left(1 - \frac{h(x, z)}{h_0} \right) dz \quad (15)$$

Substituting Eqs. (5) and (6) into Eq. (15) and considering the boundary condition $w_\alpha(w_x - l_{px}) = w_\beta(w_x - l_{px})$, there are:

$$w_\alpha = -\frac{e^2 \Delta w_x}{(9 - 2c_m)} \left[2 \left(\frac{w_x - z}{l_{px}} \right)^2 + 2 \left(\frac{w_x - z}{l_{px}} \right) + 1 \right] e^{-2 \left(\frac{w_x - z}{l_{px}} \right)} \quad (16)$$

$$w_\beta = \frac{4 \Delta w_x}{(9 - 2c_m)} \left(\frac{w_x - z}{l_{px}} - \frac{9}{4} \right) + \frac{2c_m \Delta w_x}{(9 - 2c_m)} \left[1 - \left(\frac{w_x - z}{l_{px}} \right)^4 + 2 \left(\frac{w_x - z}{l_{px}} \right)^3 - 2 \left(\frac{w_x - z}{l_{px}} \right) \right] \quad (17)$$

The above formulas satisfy the boundary condition:

$$w_\beta(x, w_x) = -\Delta w_x$$

Through further calculation, the velocity and strain rate fields in zone α and zone β are obtained:

$$\begin{cases} v_{\alpha x} = v_0 \\ v_{\alpha y} = \frac{v_0 y}{h_0} \frac{\partial h_\alpha}{\partial x} = \frac{4e^2 v_0 \tan \phi y}{(9 - 2c_m) l_{px}} \left(u^2 + 2 \frac{\Delta w_x}{l_{px}} u^2 - 2 \frac{\Delta w_x}{l_{px}} u \right) e^{-2u} \\ v_{\alpha z} = v_0 \frac{\partial w_\alpha}{\partial x} = -\frac{e^2 v_0 \tan \phi}{9 - 2c_m} \left(2u^2 + 4 \frac{\Delta w_x}{l_{px}} u^2 + 2u + 1 \right) e^{-2u} \end{cases} \quad (18)$$

$$\begin{cases} \dot{\epsilon}_{\alpha x} = 0 \\ \dot{\epsilon}_{\alpha y} = \frac{v_0}{h_0} \frac{\partial h_\alpha}{\partial x} = \frac{4e^2 v_0 \tan \phi}{(9 - 2c_m) l_{px}} \left(u^2 + 2 \frac{\Delta w_x}{l_{px}} u^2 - 2 \frac{\Delta w_x}{l_{px}} u \right) e^{-2u} \\ \dot{\epsilon}_{\alpha z} = -\frac{v_0}{h_0} \frac{\partial h_\alpha}{\partial x} = -\frac{4e^2 v_0 \tan \phi}{(9 - 2c_m) l_{px}} \left(u^2 + 2 \frac{\Delta w_x}{l_{px}} u^2 - 2 \frac{\Delta w_x}{l_{px}} u \right) e^{-2u} \end{cases} \quad (19)$$

$$\begin{cases} \dot{\epsilon}_{\alpha xy} = \dot{\epsilon}_{\alpha yx} = \frac{1}{2} \left(\frac{\partial v_x}{\partial y} + \frac{\partial v_y}{\partial x} \right) = \frac{v_0 y}{2h_0} \frac{\partial^2 h_\alpha}{\partial x^2} \\ = \frac{4e^2 v_0 \tan^2 \phi y}{(9 - 2c_m) l_{px}^2} e^{-2u} \left[2u^2 - 2u + \frac{\Delta w_x}{l_{px}} (2u^2 - 4u + 1) \right] \\ - \frac{v_0 w_{\alpha xy}''}{2h_0 \tan \phi} \frac{\partial h_\alpha}{\partial x} \\ \dot{\epsilon}_{\alpha xz} = \dot{\epsilon}_{\alpha zx} = \frac{1}{2} \left(\frac{\partial v_x}{\partial z} + \frac{\partial v_z}{\partial x} \right) = \frac{1}{2} v_0 \frac{\partial^2 w_\alpha}{\partial x^2} \\ = \frac{e^2 v_0}{18 - 4c_m} e^{-2u} \left[w_x'' (2u^2 + 2u + 1) + \frac{\Delta w_x w_{\alpha xx}'' - 2 \tan^2 \phi}{l_{px}} 4u^2 \right. \\ \left. - \frac{8 \Delta w_x \tan^2 \phi}{l_{px}^2} (u^2 - u) \right] \\ \dot{\epsilon}_{\alpha yz} = \dot{\epsilon}_{\alpha zy} = \frac{1}{2} \left(\frac{\partial v_y}{\partial z} + \frac{\partial v_z}{\partial y} \right) = \frac{v_0 y}{2h_0} \frac{\partial^2 h_\alpha}{\partial x \partial z} \\ = \frac{4e^2 v_0 \tan \phi \Delta w_x y}{(9 - 2c_m) l_{px}^3} e^{-2u} (2u^2 - 4u + 1) + \frac{4e^2 v_0 \tan \phi y}{(9 - 2c_m) l_{px}^2} e^{-2u} (u^2 - u) \end{cases} \quad (20)$$

$$\begin{cases} v_{\beta x} = v_0 \\ v_{\beta y} = \frac{v_0 y}{h_0} \frac{\partial h_\beta}{\partial x} = \frac{4c_m v_0 \tan \phi y}{(9 - 2c_m) l_{px}} \left[\frac{1}{c_m} - 2u^3 - 3u^2 + 1 + \frac{6 \Delta w_x}{l_{px}} (u^2 - u) \right] \\ v_{\beta z} = v_0 \frac{\partial w_\beta}{\partial x} = \frac{2c_m v_0 \tan \phi}{9 - 2c_m} \left[\frac{1}{c_m} \left(2u - 2 \frac{\Delta w_x}{l_{px}} - \frac{9}{2} \right) + 1 - u^4 + 2u^3 - 2u + \frac{\Delta w_x}{l_{px}} (4u^3 - 6u^2 + 2) \right] \end{cases} \quad (21)$$

$$\begin{cases} \dot{\epsilon}_{\beta x} = 0 \\ \dot{\epsilon}_{\beta y} = \frac{v_0}{h_0} \frac{\partial h_\beta}{\partial x} = \frac{4c_m v_0 \tan \phi}{(9 - 2c_m) l_{px}} \left[\frac{1}{c_m} - 2u^3 + 3u^2 - 1 + \frac{6 \Delta w_x}{l_{px}} (u^2 - u) \right] \\ \dot{\epsilon}_{\beta z} = -\frac{v_0}{h_0} \frac{\partial h_\beta}{\partial x} = -\frac{4c_m v_0 \tan \phi}{(9 - 2c_m) l_{px}} \left[\frac{1}{c_m} - 2u^3 + 3u^2 - 1 + \frac{6 \Delta w_x}{l_{px}} (u^2 - u) \right] \end{cases} \quad (22)$$

$$\begin{cases} \dot{\epsilon}_{\beta xy} = \dot{\epsilon}_{\beta yx} = \frac{1}{2} \left(\frac{\partial v_x}{\partial y} + \frac{\partial v_y}{\partial x} \right) = \frac{v_0 y}{2h_0} \frac{\partial^2 h_\beta}{\partial x^2} \\ = \frac{2c_m v_0 y}{9 - 2c_m} \left[\frac{w_x''}{l_{px}} \left(2u^3 - 3u^2 + 1 - \frac{1}{c_m} \right) - \frac{\tan^2 \phi \Delta w_x}{l_{px}^3} (12u - 6) \right. \\ \left. + \left(\frac{2 \tan^2 \phi - \Delta w_x w_x''}{l_{px}^2} \right) (6u^2 - 6u) \right] \\ \dot{\epsilon}_{\beta xz} = \dot{\epsilon}_{\beta zx} = \frac{1}{2} \left(\frac{\partial v_x}{\partial z} + \frac{\partial v_z}{\partial x} \right) = \frac{1}{2} v_0 \frac{\partial^2 w_\beta}{\partial x^2} \\ = \frac{c_m v_0}{9 - 2c_m} \left[\frac{2w_x''}{c_m} \left(-u + \frac{\Delta w_x}{l_{px}} + \frac{9}{8} \right) - 4n_2 \frac{\tan^2 \phi}{l_{px}} - w_x'' (1 - u^4 + 2u^3 - 2u) \right. \\ \left. + \frac{2 \tan^2 \phi - \Delta w_x w_{xx}''}{l_{px}} (4u^3 - 6u^2 + 2) - \frac{12 \Delta w_x \tan^2 \phi}{l_{px}^2} (u^2 - u) \right] \\ \dot{\epsilon}_{\beta yz} = \dot{\epsilon}_{\beta zy} = \frac{1}{2} \left(\frac{\partial v_y}{\partial z} + \frac{\partial v_z}{\partial y} \right) = \frac{v_0 y}{2h_0} \frac{\partial^2 h_\beta}{\partial x \partial z} \\ = \frac{12c_m v_0 \tan \phi y}{(9 - 2c_m) l_{px}^2} \left[u^2 - u - \frac{\Delta w_x}{l_{px}} (2u - 1) \right] \end{cases} \quad (23)$$

In the formulas, $u = \frac{w_x - z}{l_{px}}$.

Taking the boundary conditions in Eqs. (18) and (21), there are:

At the entrance cross section: $v_{\alpha y}(0, 0, z) = v_{\beta y}(0, 0, z) = 0$.

At the exit cross section: $v_{\alpha y}(l, y, z) = v_{\beta y}(l, y, z) = 0$,
 $v_{\alpha z}(l, y, z) = v_{\beta z}(l, y, z) = 0$.

At the boundary of zone α and zone β :
 $v_{\alpha x}(x, y, w_x - l_{px}) = v_{\beta x}(x, y, w_x - l_{px}) = v_0$

$v_{\alpha y}(x, y, w_x - l_{px}) = v_{\beta y}(x, y, w_x - l_{px})$

$v_{\alpha z}(x, y, w_x - l_{px}) = v_{\beta z}(x, y, w_x - l_{px})$

According to Eqs. (19) and (22), the incompressible property is satisfied:

$$\dot{\epsilon}_{\alpha x} + \dot{\epsilon}_{\alpha y} + \dot{\epsilon}_{\alpha z} = 0, \dot{\epsilon}_{\beta x} + \dot{\epsilon}_{\beta y} + \dot{\epsilon}_{\beta z} = 0$$

2.4 Total Power Functional

The total power functional of vertical rolling process is obtained by using the first variation principle of rigid-plastic material:

$$J^* = N_i + N_s + N_f \quad (24)$$

where N_i , N_s and N_f represent plastic deformation power, shear power and friction power, respectively.

Based on Mises yield criterion, the plastic deformation power is:

$$\begin{aligned} N_i &= \iiint_V D(E_{ij}) dV = \sqrt{\frac{2}{3}} \sigma_s \iiint_V \sqrt{\dot{\epsilon}_{ij} \dot{\epsilon}_{ij}} dV \\ &= \frac{4\sqrt{6}}{3} \sigma_s \int_0^l \int_0^{w_x - l_{px}} \int_0^{h_\alpha} \sqrt{\dot{\epsilon}_{\alpha x}^2 + \dot{\epsilon}_{\alpha y}^2 + \dot{\epsilon}_{\alpha z}^2 + 2\dot{\epsilon}_{\alpha xy}^2 + 2\dot{\epsilon}_{\alpha xz}^2 + 2\dot{\epsilon}_{\alpha yz}^2} dydzdx \\ &\quad + \frac{4\sqrt{6}}{3} \sigma_s \int_0^l \int_{w_x - l_{px}}^{w_x} \int_0^{h_\beta} \sqrt{\dot{\epsilon}_{\beta x}^2 + \dot{\epsilon}_{\beta y}^2 + \dot{\epsilon}_{\beta z}^2 + 2\dot{\epsilon}_{\beta xy}^2 + 2\dot{\epsilon}_{\beta xz}^2 + 2\dot{\epsilon}_{\beta yz}^2} dydzdx \end{aligned} \quad (25)$$

At the exit section, there is no shear power because of the continuous velocity field. At entrance section, the discontinuity of velocity exists and the shear power can be expressed as:

$$N_s = \int_{S_0} \tau_s |\Delta v_s| dS = 4\tau_s \int_0^{w_0} \int_0^{h_0} \sqrt{(v_y|_{x=0})^2 + (v_z|_{x=0})^2} dydz \quad (26)$$

where $\tau_s = \sigma_s / \sqrt{3}$ is the shear yield stress.

In vertical rolling process, the plastic deformation and the relative motion between roller and slab lead to extremely complicated tangential force and displacement on the contact interface. In the 3D rolling model proposed by Lian et al. (1984), the contact surface is divided into sliding zone and deformation stagnation zone (adhesion zone).

There is an initial displacement of sliding friction on the contact interface. Only when the calculated velocity discontinuity Δv_f becomes larger than the initial velocity discontinuity Δv_c , the sliding and the friction power exist. The friction shear stress in the adhesive zone is assumed to be proportional to the displacement as:

$$\tau_f = m\tau_s \frac{\Delta v_f}{\Delta v_c} \quad (27)$$

According to the empirical formula obtained from the experiments of hot plain rolling (Shchepinsky 1987), the length of adhesion zone is given by:

$$l_c = 0.2mRl \quad (28)$$

For plain rolling, the adhesion zone is located on both sides of the neutral point. Differently in vertical rolling, the linear velocity of the roller surface is consistent with the rolling speed of the slab. From the above principle, the point with the same velocity of vertical roller and slab is located at the exit section, that is, the adhesion zone only exists on

single side of the neutral point. So, the length of adhesion zone can be rewritten as:

$$l_c = 0.1mRl \quad (29)$$

In the sliding zone, the friction factor is constant and the friction shear stress is:

$$\tau_f = m\tau_s \quad (30)$$

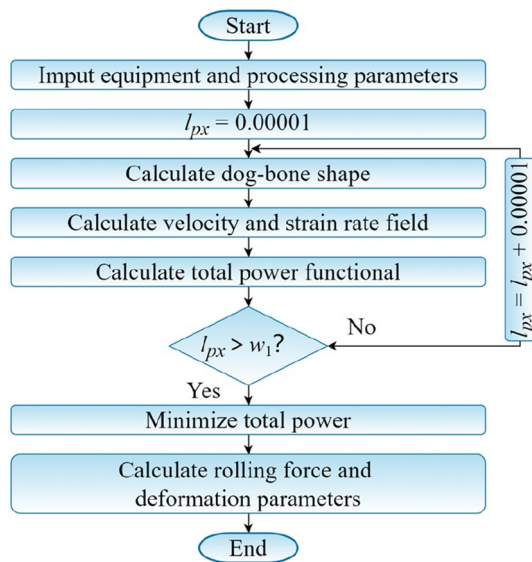


Fig. 4 Flowchart of the calculation

On the sliding interface, the friction shear stress and the velocity discontinuity are collinear vectors. The friction power is:

$$N_f = \int_{S_f} |\tau_f| |\Delta v_f| \cos(\tau_f, \Delta v_f) ds \tag{31}$$

$$= 4m\tau_s \int_0^{l-l_c} \int_0^{h_{rx}} \sqrt{(v_y|_{z=w_x})^2 + \Delta v_t^2} \sec \phi dy dx$$

where $\Delta v_t = \frac{v_0}{\cos \phi} - v_R$ is the tangential velocity discontinuity on the interface.

Substituting Eqs. (25), (26) and (31) into Eq. (24), the expression of total power functional changes into:

$$J^* = \frac{4\sqrt{6}}{3} \sigma_s \int_0^l \int_0^{w_x-l_{px}} \int_0^{h_a} \sqrt{\dot{\epsilon}_{ax}^2 + \dot{\epsilon}_{ay}^2 + \dot{\epsilon}_{az}^2 + 2\dot{\epsilon}_{axy}^2 + 2\dot{\epsilon}_{axz}^2 + 2\dot{\epsilon}_{ayz}^2} dy dz dx$$

$$+ \frac{4\sqrt{6}}{3} \sigma_s \int_0^l \int_{w_x-l_{px}}^{w_x} \int_0^{h_b} \sqrt{\dot{\epsilon}_{\beta x}^2 + \dot{\epsilon}_{\beta y}^2 + \dot{\epsilon}_{\beta z}^2 + 2\dot{\epsilon}_{\beta xy}^2 + 2\dot{\epsilon}_{\beta xz}^2 + 2\dot{\epsilon}_{\beta yz}^2} dy dz dx \tag{32}$$

$$+ 4\tau_s \int_0^{w_0} \int_0^{h_0} \sqrt{(v_y|_{x=0})^2 + (v_z|_{x=0})^2} dy dz + 4\tau_f \int_0^{l-l_c} \int_0^{h_{rx}} \sqrt{(v_y|_{z=w_x})^2 + \Delta v_t^2} \sec \phi dy dx$$

The calculation procedure of energy model is shown in Fig. 4. When known the geometry size and movement speed of steel slab and rollers, the physical parameters of material, the width reduction and the friction factor, the total power functional are defined by the only undetermined constant

parameter l_{px} (Zhang 2016). Continuously changing the unknown parameter l_{px} , numerical calculation is carried out by using MATLAB to solve the corresponding total power functional until $l_{px} = w_1$. The minimum of total power J_{min}^* is selected as the actual solution based on minimum energy principle. The rolling torque M and the rolling force per unit slab thickness F_0 are determined by the following equation (Zhang et al. 2014):

$$J_{min}^* = 2M \frac{v_R}{R} = 4h_0 l \chi F_0 \omega_V \tag{33}$$

where χ is the arm factor. In this paper, it is selected as 0.44 (Qi and Wang 2012).

3 Numerical Research

3.1 Validation of the Model

The dog-bone shape at outlet predicted by the presented model is compared with several results. As shown in Fig. 5a, the presented model predicted a lower and wider dog-bone than sine (Liu et al. 2015) and double parabolic (Liu et al. 2016) function model. The presented shape is more uniform than that of global weighted model (Yang et al. 2022), which seems that the global weighted velocity field is not very applicable when the width reduction is small. The predicted length of dog-bone is closer to the value predicted by Yun et al. (2012). Compared with other theoretical and fitted (Okado et al. 1981; Xiong et al. 1997) results in Fig. 5c, the dog-bone peak position (l_{px}) obtained by presented model is closer to the experimental result (Shibahara et al. 1981) with a less error of h_r/h_b value (within 0.5%). In addition, the presented curve is more accurate in describing the end

part of dog-bone deformation, and the calculated length of plastic deformation zone (l_{bx}) is rather credible. However, the predicted height of dog-bone peak is higher than the other result. This is due to the assumption of plane deformation, which neglects the metal flow along rolling direction.

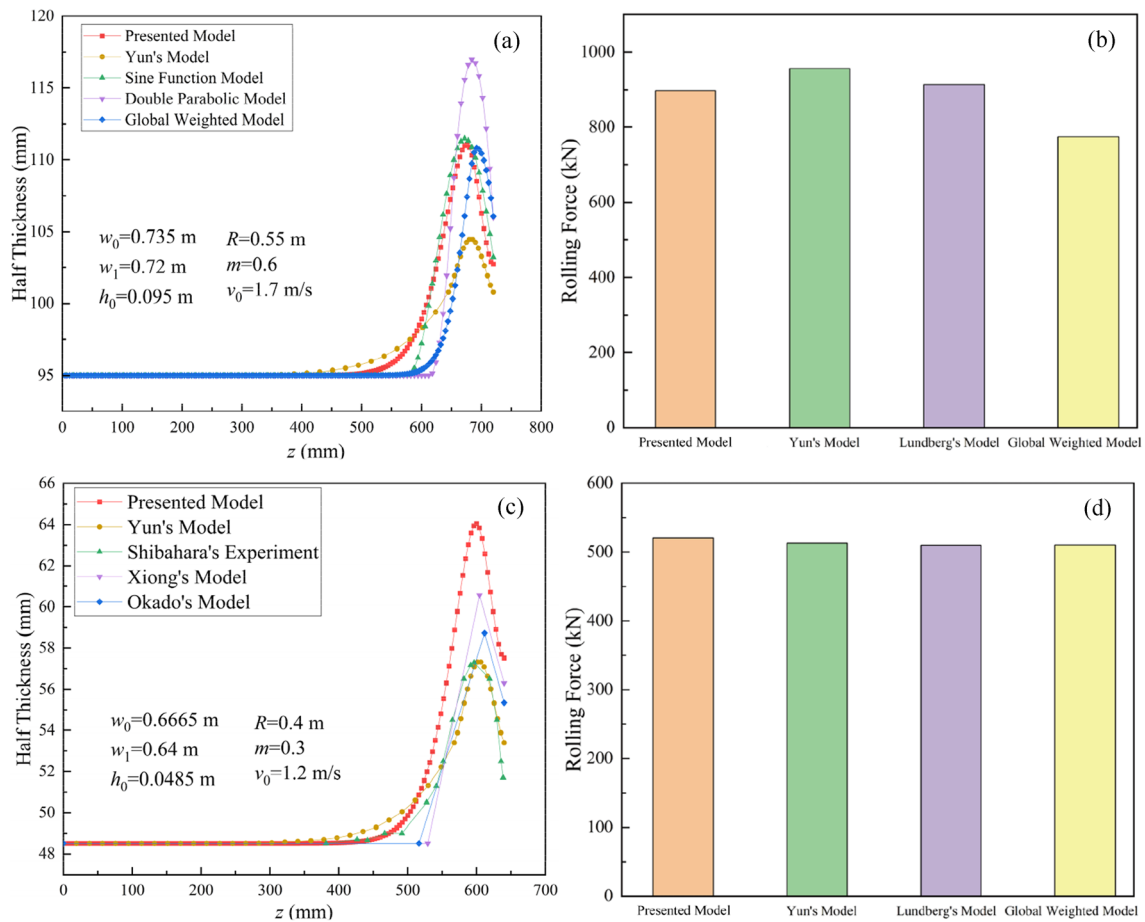


Fig. 5 Comparison of edge shape and rolling force predicted by several models

The comparison of rolling force shows that the calculated values are very close to the results obtained by Yun et al. (2012) and Lundberg (2008), and the error is less than 7%. In Fig. 5b, when the width reduction rate is small, the predicted rolling force of global weighted model is sharply smaller than other results. It seems that the presented model is more reasonable.

It is effective to validate the theoretical model through experiments (Bari and Kumar 2023a, b). The vertical rolling experiments are performed on a small rolling mill in laboratory. The radius of vertical rollers is 50 mm. Pressure sensors are installed at the vertical rollers on both sides, respectively, to measure the total rolling force. Heavy strain hardened copper specimens and precipitation hardened aluminum specimens are selected as experimental material. By continuous casting, the materials are made into 25-mm thick plates, and then cold rolled to 8 and 6 mm to avoid strain

Table 1 Parameters of materials and processes

Materials	Shear yield stress τ_s (MPa)	Half of thickness h_0 (mm)	Width reduction rate $\Delta w/w_0$ (%)
Cu	217	4.275	1.83
		4.3	1.83
		4.2	2.17
		4.2	2.67
Cu	181	3.095	3.58
		3.125	3.67
		3.13	3.83
		3.1	4.25
Al	170	2.975	2.5
		3.025	4.08

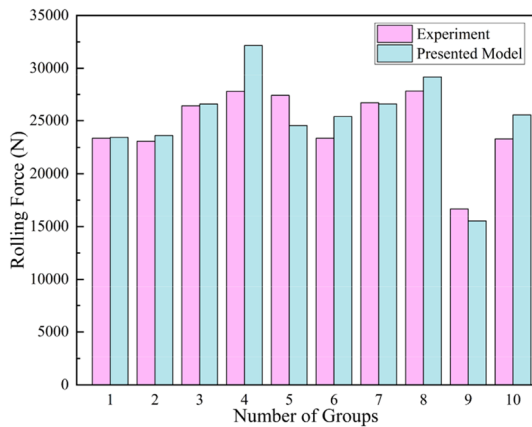


Fig. 6 Comparison of rolling force obtained by presented model and measurement

hardening during further deformation. And thus, it would be approximately ideally plastic during edge rolling experiment. The length and width of slabs are 300 mm and 60 mm, respectively. The shear yield strength of the materials was determined by a simple tensile test (EN 10002) (Lundberg 1993;2008).

When the width reduction rate is selected between 1.8 and 4.25%, the rolling force predicted by the presented model is compared with 10 groups of experiments (Li et al. 2016). Table 1 shows the mechanics and process parameters of the experimental materials. Figure 6 shows that the total error of the presented values compared with measurements is less than 14%. When the width reduction rate is small, the presented model performs better. As the width reduction rate increasing, the numerical results become slightly higher than the experimental values, which can be explained that the plane deformation assumption ($v_x = v_0$) predicted a bigger edge deformation.

3.2 Dog-bone deformation

Based on the above calculation method, the edge deformation was calculated with the value of $\frac{\Delta w}{w_0} = 0.01 - 0.05$, $\frac{h_0}{w_0} = 0.08 - 0.16$, $\frac{R}{w_0} = 0.65 - 1.05$, $m = 0.3 - 0.7$. The relationship between the cross section of dog-bones at outlet and the rolling parameters is shown in Fig. 7. The predicted peak position is compared with the results predicted by Xiong et al. (1997). All the parameters were non-dimensionalized. In the study of width reduction rate, thickness, width and roller radius, the friction factors are given as 0.3 (Byon et al. 2018) uniformly.

Figure 7a shows that with the width reduction rate increasing, the deformation zone becomes larger and extends obviously. Accordingly, h_b and h_r increase as well as the dog-bone peak moves inward. The influence

of initial thickness is similar to width reduction rate, as shown in Fig. 7c and d. The increase of initial thickness enlarges the deformation extent and area, which let l_b and l_p linear rise approximately. It is worth to note that in Fig. 7e, with the decrease of h_0/w_0 , h_r/h_0 and h_b/h_0 rise, while the peak moves outward, which indicates that the deformation will be more concentrated at the edge. In other words, it will aggravate the non-uniform deformation. The deformation area extends inward slightly and the peak has a small decrease with the increase of vertical roller radius, as Fig. 7g and h shown. The expansion of the interface will enhance the resistance along rolling direction, and the movement tendency toward the center of width becomes stronger. It can be seen in Fig. 7i and j that the effect of friction factor on dog-bone deformation is limited and mainly concentrated in zone β .

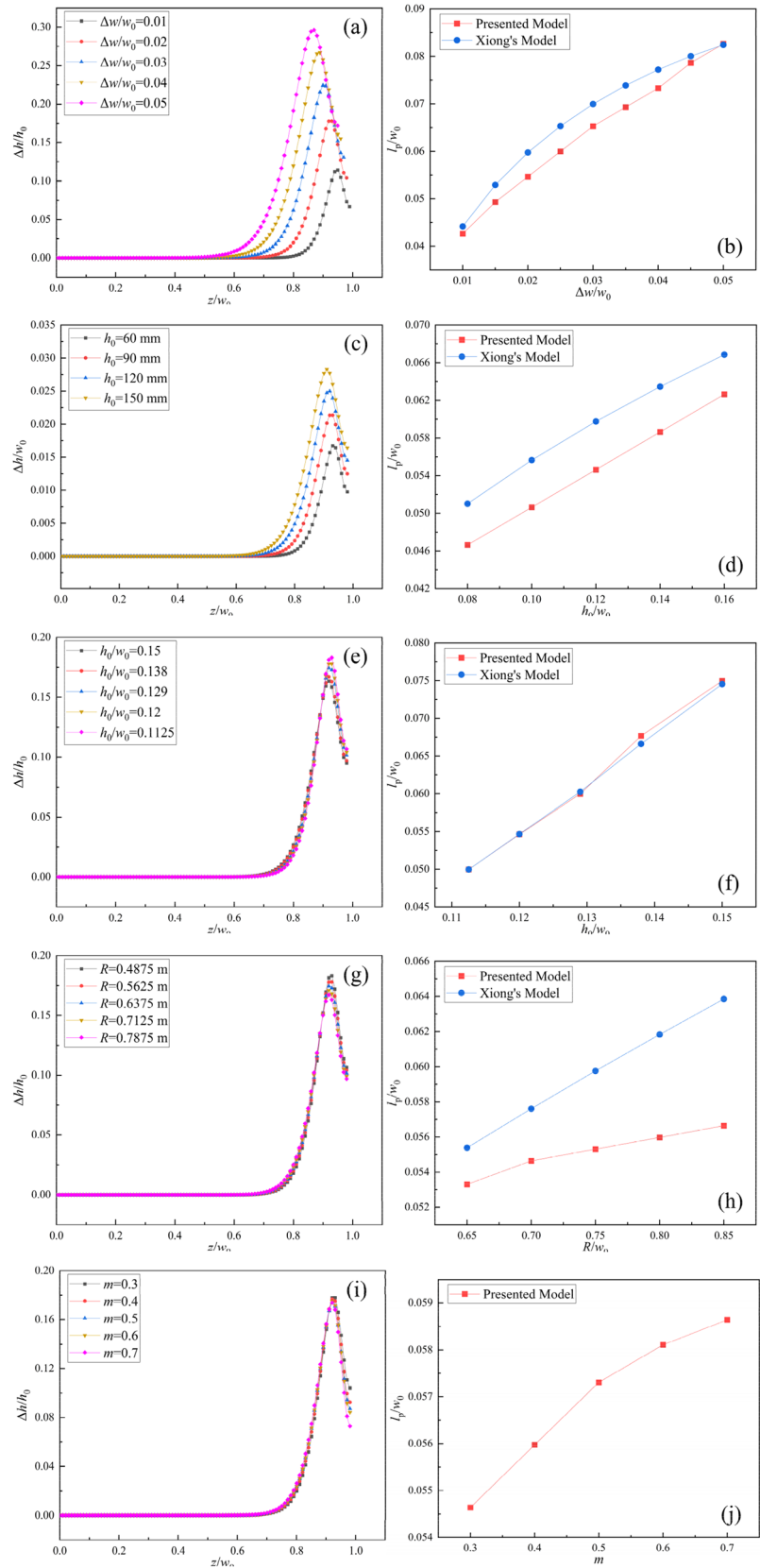
3.3 Rolling Power and Rolling Force

The comparison of presented function model and sine DSF Model (Liu et al. 2018) in the proportion of three kinds of power in total power is exhibited in Fig. 8. It can be seen that plastic deformation power is dominant (more than 60%). The second one is shear power, and friction power is the minimum. Further analysis found that the presented model predicted a less proportion of friction power, which can be attributed to the consideration of adhesion zone. The comparison model assumes that the entire contact interface is in sliding condition and generates friction power while in the presented model, the adhesion within the contact zone is considered. In the adhesion zone, there is no sliding; thus, no friction power exists, which results in a smaller predicted friction power (Lian et al. 1984; Chen et al. 2018).

Figure 9 shows the ratio of several power in total power varies with rolling parameters. In Fig. 9a, with the increase of width reduction rate, plastic deformation zone becomes larger, while the increase of the entrance shear plane and the contact interface is smaller. So, the proportion of plastic deformation power increases obviously. The increase of slab thickness sharply enlarges the contact interface and the entrance shear plane, which increases the proportion of friction power and shear power, as shown in Fig. 9b. From Fig. 9c, the increase of radius makes the deformation expands slightly to the width center, resulting in a minor increase of deformation power. As shown in Fig. 9d, the growth of friction factor increases the friction power, while the proportion of deformation power and shear power changes slightly.

The change of rolling force with rolling parameters is shown in Fig. 10. The increase of width reduction rate and slab thickness cause the expansion of deformation region and the obvious rise of rolling force, as Fig. 10a and b shows, respectively. As shown in Fig. 10c, the increase of

Fig. 7 Effects of **a**, **b** $\Delta w/w_0$
c, **d** h_0 **e**, **f** h_0/w_0 **g**, **h** R **i**, **j** m
 on dog-bone shape and peak position



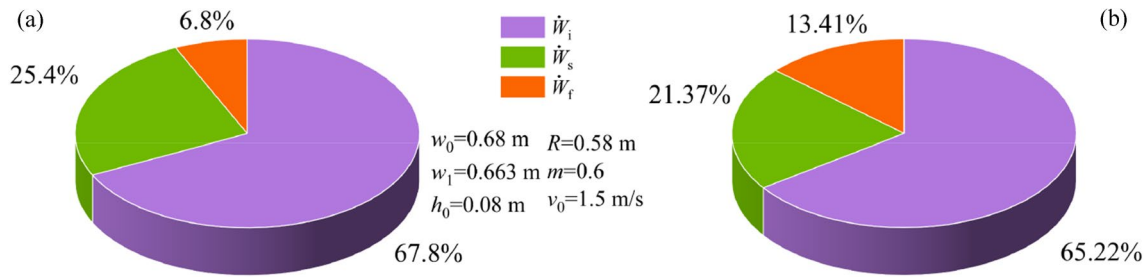


Fig. 8 The proportion of powers calculated by a presented model and b sine DSF model

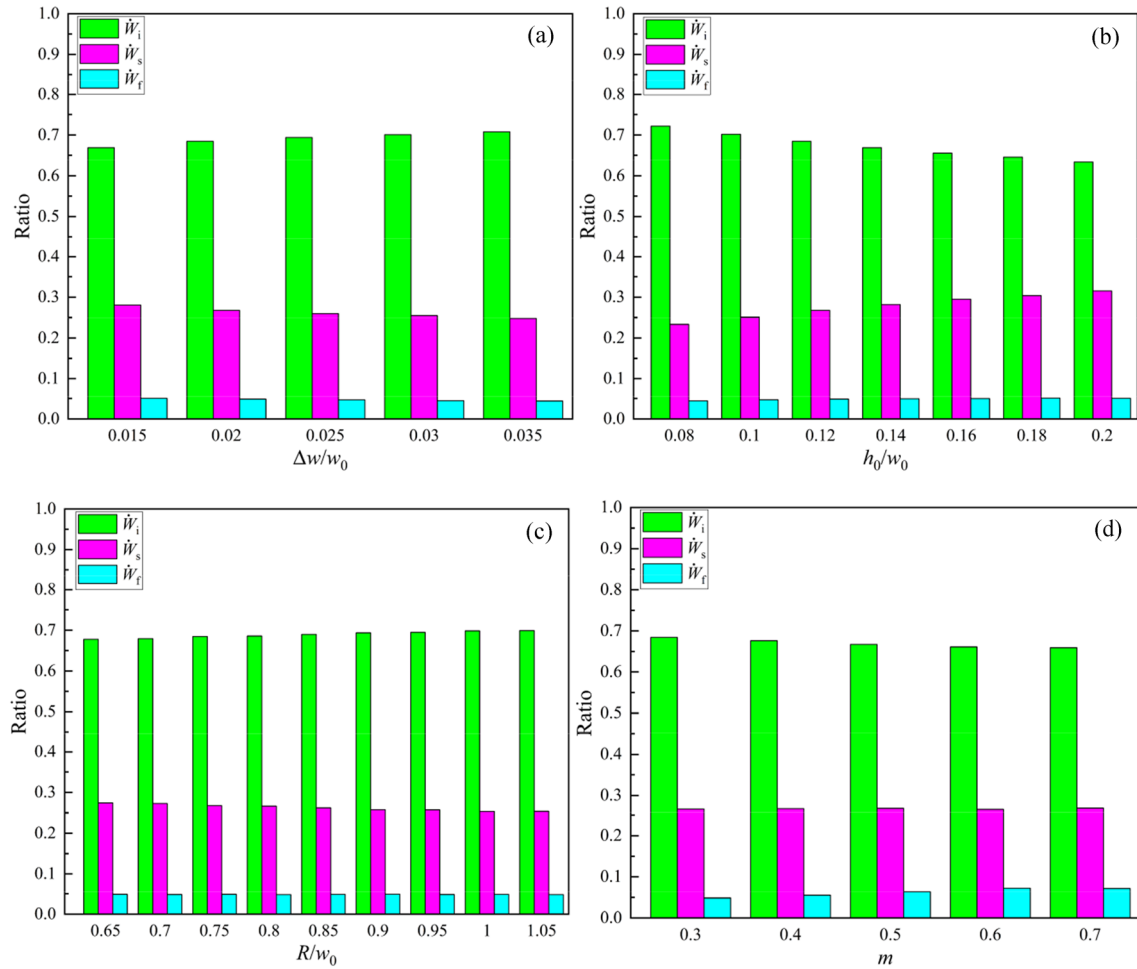


Fig. 9 Effects of a $\Delta w/w_0$ b h_0 c R d m on power ratio in total power

vertical roller radius expands the deformation zone and the contact interface, which result in a minor increase of rolling force. In Fig. 10d, the increase of friction factor leads to a growth of rolling force. However, the change range of rolling force is tiny, which can be attributed to the limited proportion of friction power in total power.

4 Conclusions

1. This is a crossover study on both mathematic and mechanics. Based on the incompressibility and rigid–plastic of the steel slab, a combination of theory and engineering is carried out to analyze the vertical rolling

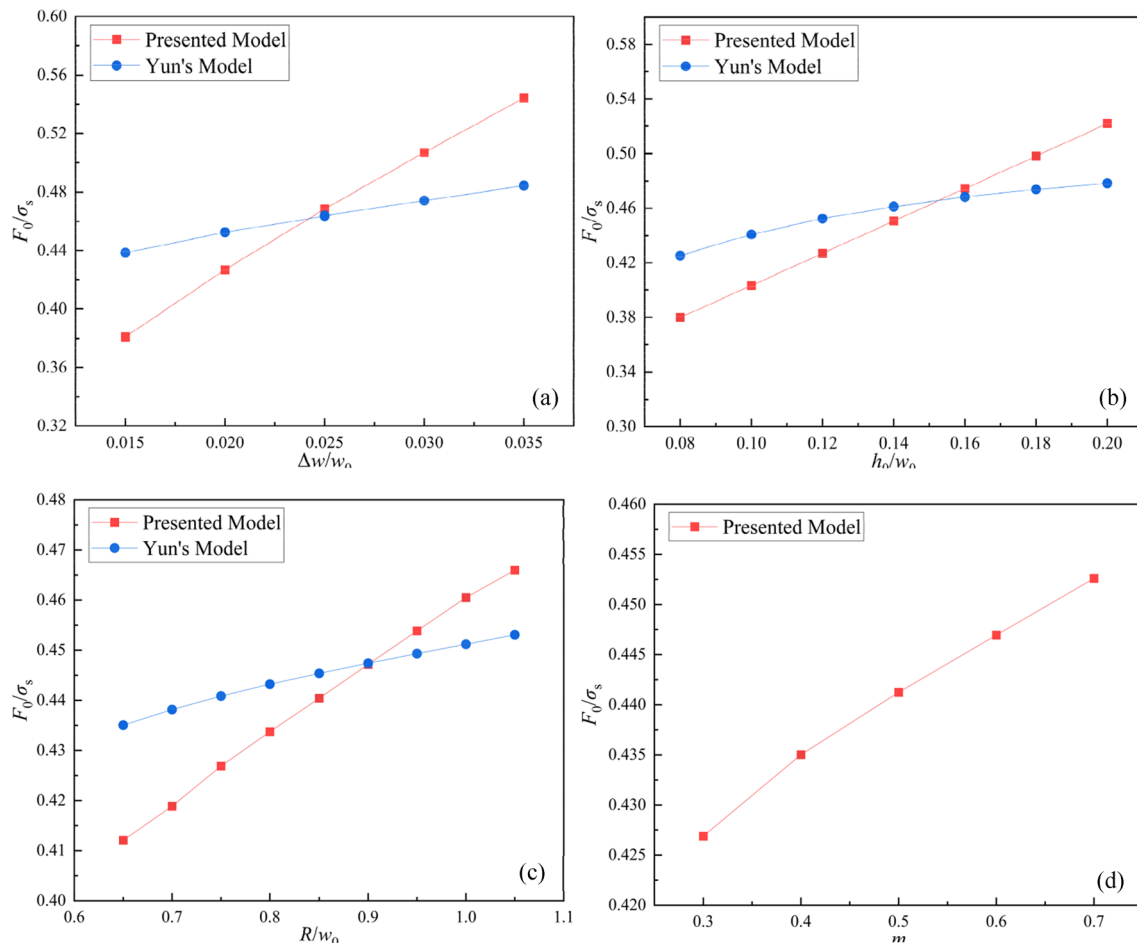


Fig. 10 Effects of **a** $\Delta w/w_0$ **b** h_0/w_0 **c** R/w_0 **d** m on rolling force

process. A new model called gamma distribution–cubic function dog-bone model is put forward and the velocity and strain rate fields are derived according to stream function method. According to the first variation principle of rigid–plastic material and fully considering the adhesion and sliding of the friction interface, the total power functional is given. The proposed model can be applied for accurate prediction of the dog-bone deformation at the edge and rolling force.

- The developed method is compared with several models and the reliability is well verified by experiment results. On this basis, the influences of several process parameters on rolling power, rolling force and dog-bone shape are discussed. The increase of slab thickness and width reduction rate leads to a significant expansion of edge deformation. The height of dog-bone decreases and moves inward, which can lighten the non-uniform edge deformation by increasing the ratio of thickness to width or changing the rollers with larger radius. The effect of friction factor on dog-bone shape is slight. Plastic deformation power accounts for

the largest proportion in total power, and friction power accounts for the least. The width reduction rate and initial slab thickness have considerable impacts on power proportion and rolling force. By comparison, the effects of vertical roller radius and friction factor are rather smaller.

Author Contributions All authors contributed to the study conception and design. Material preparation and data collection and analysis were performed by BY. The first draft of the manuscript was written by BY. All authors commented on previous versions of the manuscript. All authors read and approved the final manuscript.

Funding The authors declare that no funds, grants, or other support was received during the preparation of this manuscript.

Availability of Data and Material The authors assure the transparency and availability of data and material and adhere to discipline-specific rules for acquiring, selecting and processing data.

Code Availability The authors make sure we have permissions for the use of software, and the availability of the custom code.

Declarations

Conflict of interest The authors have no relevant financial or non-financial interests to disclose.

Ethics Approval The authors declare that the submitted work is original. Neither the entire paper nor any part of its content has been published or has been accepted elsewhere. It is not being submitted to any other journal.

Consent to Participate The authors confirm that this research does not involve Human Participants and/or Animals.

Consent for Publication The authors consent for publication in *Iranian Journal of Science and Technology, Transactions of Mechanical Engineering* exclusively.

References

- Bari N, Kumar S (2023a) Multi-stage single-point incremental forming: an experimental investigation of thinning and peak forming force. *J Braz Soc Mech Sci*. <https://doi.org/10.1007/s40430-023-04055-7>
- Bari N, Kumar S (2023b) Multi-stage single-point incremental forming: an experimental investigation of surface roughness and forming time. *J Mater Eng Perform* 32:1369–1381. <https://doi.org/10.1007/s11665-022-07183-8>
- Byon SM, Lee HJ, Lee Y (2018) Finite element-based inverse approach to estimate the friction coefficient in hot bar rolling process. *Proc Inst Mech Eng Part B J Eng Manuf* 232(11):1996–2007. <https://doi.org/10.1177/0954405416683428>
- Cao JZ, Liu YM, Luan FJ, Zhao DW (2016) The calculation of vertical rolling force by using angular bisector yield criterion and Pavlov principle. *Int J Adv Manuf Tech* 86(9–12):2701–2710. <https://doi.org/10.1007/s00170-016-8373-2>
- Chen CC, He AR, Gao L, Guo DF (2018) Research on rapid online calculation method of three-dimensional plastic deformation. *Control Eng China* 25(5):777–783. <https://doi.org/10.14107/j.cnki.kzgc.160573>
- Forouzan MR, Salehi I, Adibi-sedeh AHA (2009) Comparative study of slab deformation under heavy width reduction by sizing press and vertical rolling using FE analysis. *J Mater Process Technol* 209(2):728–736. <https://doi.org/10.1016/j.jmatprotec.2008.02.063>
- Ginzburg VB, Kaplan N, Bakhtar F, Tabone CJ (1991) Width control in hot strip mills. *Iron Steel Eng* 68(6):25–39
- Huisman HJ, Huëtink J (1985) A combined eulerian–lagrangian three-dimensional finite–element analysis of edge–rolling. *J Mech Work Technol* 11(3):333–353
- Li X, Wang H, Liu Y, Zhang DH (2016) Analysis of edge rolling based on continuous symmetric parabola curves. *J Braz Soc Mech Sci* 39(4):1–10. <https://doi.org/10.1007/s40430-016-0587-6>
- Lian JC, Duan ZY, Ye X (1984) Analysis of metal transverse flow in roll gap with three–dimensional finite difference method. *J North-east Heavy Mach Inst* 20(3):1–9
- Liu YM, Ma GS, Zhang DH, Zhao DW (2015) Upper bound analysis of rolling force and dog–bone shape via sine function model in vertical rolling. *J Mater Process Technol* 223:91–97. <https://doi.org/10.1016/j.jmatprotec.2015.03.051>
- Liu YM, Zhang DH, Zhao DW, Sun J (2016) Analysis of vertical rolling using double parabolic model and stream function velocity field. *Int J Adv Manuf Tech* 82(5–8):1153–1161. <https://doi.org/10.1007/s00170-015-7393-7>
- Liu YM, Sun J, Zhang DH, Zhao DW (2018) Three–dimensional analysis of edge rolling based on dual–stream function velocity field theory. *J Manuf Process* 34:349–355
- Liu YM, Hao PJ, Wang T, Run ZK, Sun J, Zhang DH, Zhang SH (2020) Mathematical model for vertical rolling deformation based on energy method. *Int J Adv Manuf Tech* 107(1–2):875–883. <https://doi.org/10.1007/s00170-020-05094-3>
- Liu YM, Wang ZH, Wang T, Sun J, Hao JP, Zhang DH, Huang QX (2022) Prediction and mechanism analysis of the force and shape parameters using cubic function model in vertical rolling. *J Mater Process Technol* 303:117500. <https://doi.org/10.1016/j.jmatprotec.2022.117500>
- Lundberg SE (1986) An approximate theory for calculation of roll torque during edge rolling of steel slabs. *Steel Res Int* 57(7):325–330. <https://doi.org/10.1002/srin.198600773>
- Lundberg SE (2008) A model for prediction of roll force and torque in edge rolling. *Steel Res Int* 78(2):160–166. <https://doi.org/10.1002/srin.200705874>
- Lundberg SE, Gustafsson T (1993) Roll force, torque, lever arm coefficient, and strain distribution in edge rolling. *J Mater Eng Perform* 2(6):873–879. <https://doi.org/10.1007/BF02645688>
- Okado M, Ariizumi T, Noma Y, Yabuuchi K, Yamazaki Y (1981) Width behaviour of the head and tail of slabs in edge rolling in hot strip mills. *Tetsu Hagane* 67(15):2516–2525
- Qi KM, Wang YP (2012) Metal plastic processing—rolling theory and technology. Metallurgical Industry Press, Beijing
- Ruan JH, Zhang LW, Gu SD, He WB, Chen SH (2014) 3D FE modeling of plate shape during heavy plate rolling. *Ironmak Steelmak* 41(3):199–205. <https://doi.org/10.1179/1743281213Y.000000119>
- Shchepinsky W (1987) Introduction to metal plastic forming mechanics. Mechanical Industry Press, Beijing
- Shibahara T, Misaka Y, Kono T, Koriki M, Takemoto H (1981) Edger set–up model at roughing train in hot strip mill. *Tetsu Hagane* 67(15):2509–2515. https://doi.org/10.2355/tetsuhagane1955.67.15_2509
- Tazoe N, Honjyo H, Takeuchi M, Ono T (1984) New form of hot strip mill width rolling installations. In: AISE spring conference. Dearborn, Assn Iron Steel Engineers, Pittsburgh, pp 85–88
- Xiong SW, Zhu XL, Liu XH, Wang G, Zhang Q, Li H, Meng X, Han L (1997) Mathematical model of width reduction process of roughing trains of hot strip mills. *Shanghai Met* 19:39–43
- Xiong SW, Rodrigues JMC, Martins PAF (2003) Three–dimensional modelling of the vertical–horizontal rolling process. *Finite Elem Anal Des* 39(11):1023–1037. [https://doi.org/10.1016/S0168-874X\(02\)00154-3](https://doi.org/10.1016/S0168-874X(02)00154-3)
- Yang BX, Xu HJ, An Q (2022) Analysis of 3D plastic deformation in vertical rolling based on global weighted velocity field. *Int J Adv Manuf Tech* 120:6647–6659. <https://doi.org/10.1007/s00170-022-09190-4>
- Yun D, Lee D, Kim J, Hwang SM (2012) A new model for the prediction of the dog–bone shape in steel mills. *ISIJ Int* 52(6):1109–1117. <https://doi.org/10.2355/isijinternational.52.1109>
- Zhang SH (2016) Mechanical principle of plastic forming. Metallurgical Industry Press, Beijing
- Zhang DH, Cao JZ, Xu JJ, Peng W, Zhao DW (2014) Simplified weighted velocity field for prediction of hot strip rolling force by taking into account flattening of rolls. *J Iron Steel Res Int* 21(7):637–643. [https://doi.org/10.1016/S1006-706X\(14\)60099-6](https://doi.org/10.1016/S1006-706X(14)60099-6)
- Zhang YF, Zhang HY, Chen LJ, Zhao DW, Zhang DH (2018) Calculation of vertical rolling force through slip–line field. *J Plast Eng*

25(6):288–291. <https://doi.org/10.3969/j.issn.1007-2012.2018.06.042>

Zhang YF, Di HS, Li X, Zhao DW, Zhang DH (2020) Combined analysis of vertical rolling force with slab method and slip–line field. *J Plast Eng* 27(1):153–158. <https://doi.org/10.3969/j.issn.1007-2012.2020.01.021>

Springer Nature or its licensor (e.g. a society or other partner) holds exclusive rights to this article under a publishing agreement with the author(s) or other rightsholder(s); author self-archiving of the accepted manuscript version of this article is solely governed by the terms of such publishing agreement and applicable law.